Supporting Information

2D Hybrid Superlattice-Based On-Chip Electrocatalytic Microdevice for *In Situ* Revealing Enhanced Catalytic Activity

Yabin Guo,[†] Qiao Chen,[§] Anmin Nie,[‡] Huan Yang,[†] Wenbin Wang,[†] Jianwei Su,[†] Shuzhe Wang,[†] Youwen Liu,*[,†] Shun Wang,[§] Huiqiao Li,[†] Zhongyuan Liu,[‡] and Tianyou Zhai*[,†]

[†] State Key Laboratory of Material Processing and Die & Mould Technology, School of Materials Science and Engineering, Huazhong University of Science and Technology, Wuhan, Hubei, 430074, P. R. China

[‡] State Key Laboratory of Metastable Materials Science and Technology, Yanshan University, Qinhuangdao, Hebei, 066004, P. R. China

[§] MOE Key Laboratory of Fundamental Physical Quantities Measurements, School of Physics, Huazhong University of Science and Technology, Wuhan, Hubei, 430074, P. R. China

Corresponding Author

* zhaity@hust.edu.cn; ywliu@hust.edu.cn

S1. Atomic structure information of 2H-TaS_2 single crystal and flakes.

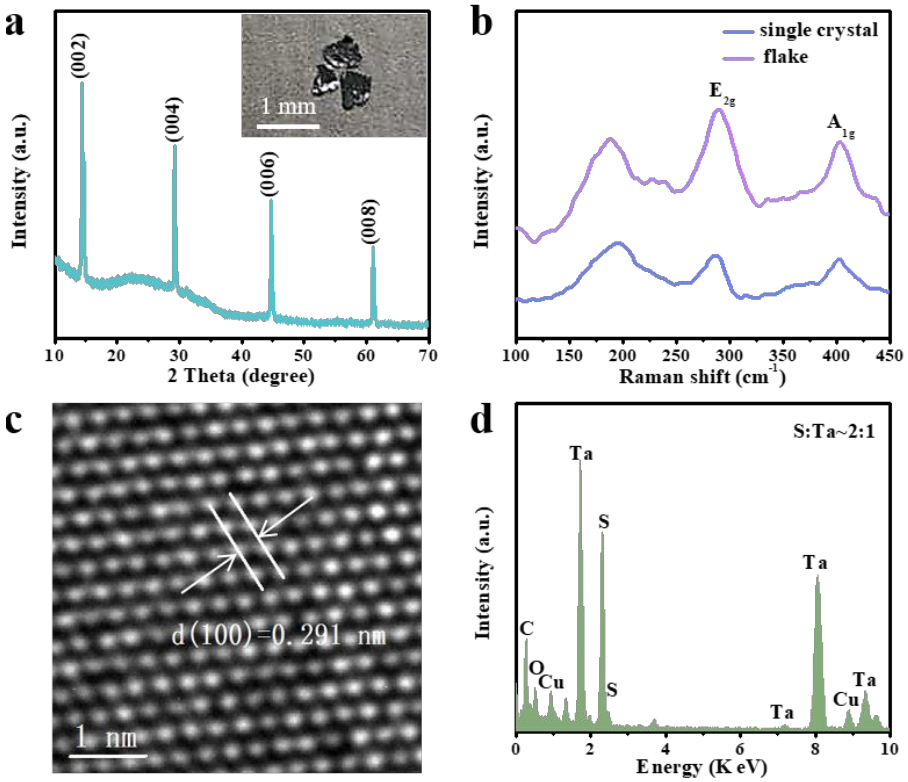

Figure S1. Atomic structure information of 2H-TaS_2 single crystal and flakes. (a) XRD pattern for a 2H-TaS_2 single crystal. Inset are images of single crystal flakes with centimeter size. (b) Raman spectra. (c, d) HRTEM of an exfoliated flake and its corresponding EDS. The XRD pattern of the single crystal obtained by CVT can be well identified to the P63/mmc space group and the diffraction peak shows preferential orientation along the [001] crystal axis. The distinct photon modes at 403.26 cm^{-1} (A_{1g}) and 284.08 cm^{-1} (E^1_{2g}) are characteristic of 2H-TaS_2 nanosheet. The HRTEM image confirms the atomic arrangement of 2H-TaS_2 and the interplanar spacing of 0.291 nm corresponds to (001) crystal face. EDS spectra shows the compositional information of the exfoliated flake with ratio of Ta and S elements closing to 1:2.

S2. Optical micrographs corresponding to fresh, intercalation, and annealing state of TaS_2 nanosheets.

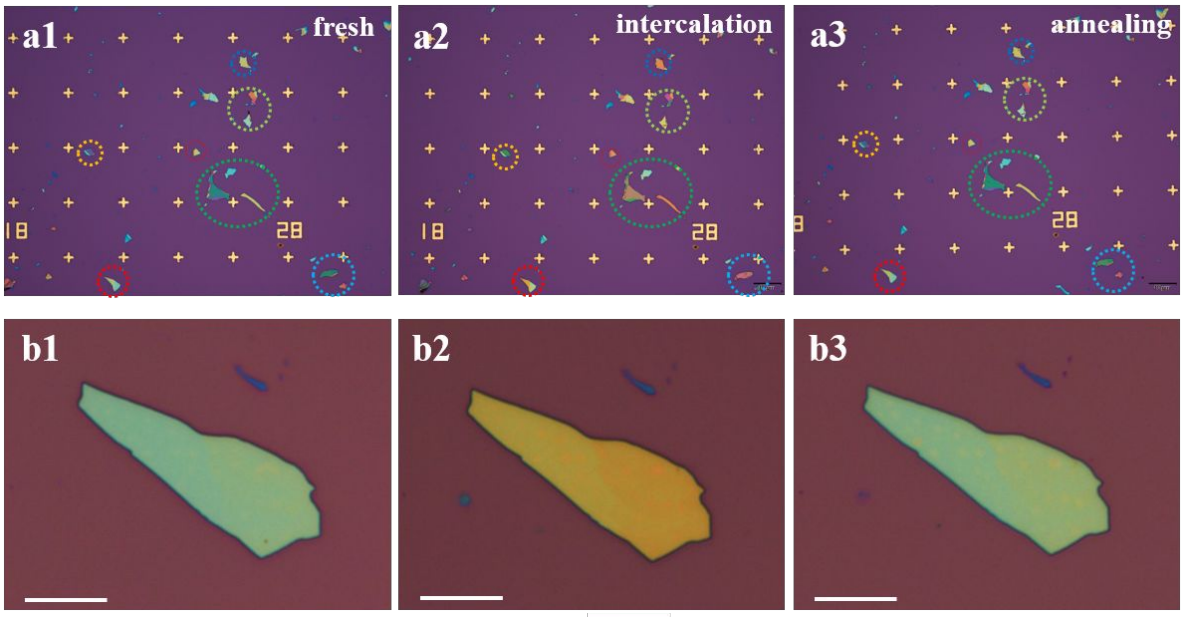

Figure S2. Optical micrographs corresponding to fresh, intercalation, and annealing state of TaS_2 nanosheets. (a1, a2, a3) Different size of TaS_2 nanosheets showing the similar change in color. (b1, b2, b3) Another individual nanosheet. Scale bar, 10 μm.

S3. Optical micrographs corresponding to fresh and intercalation state of TaS_2 nanosheets.

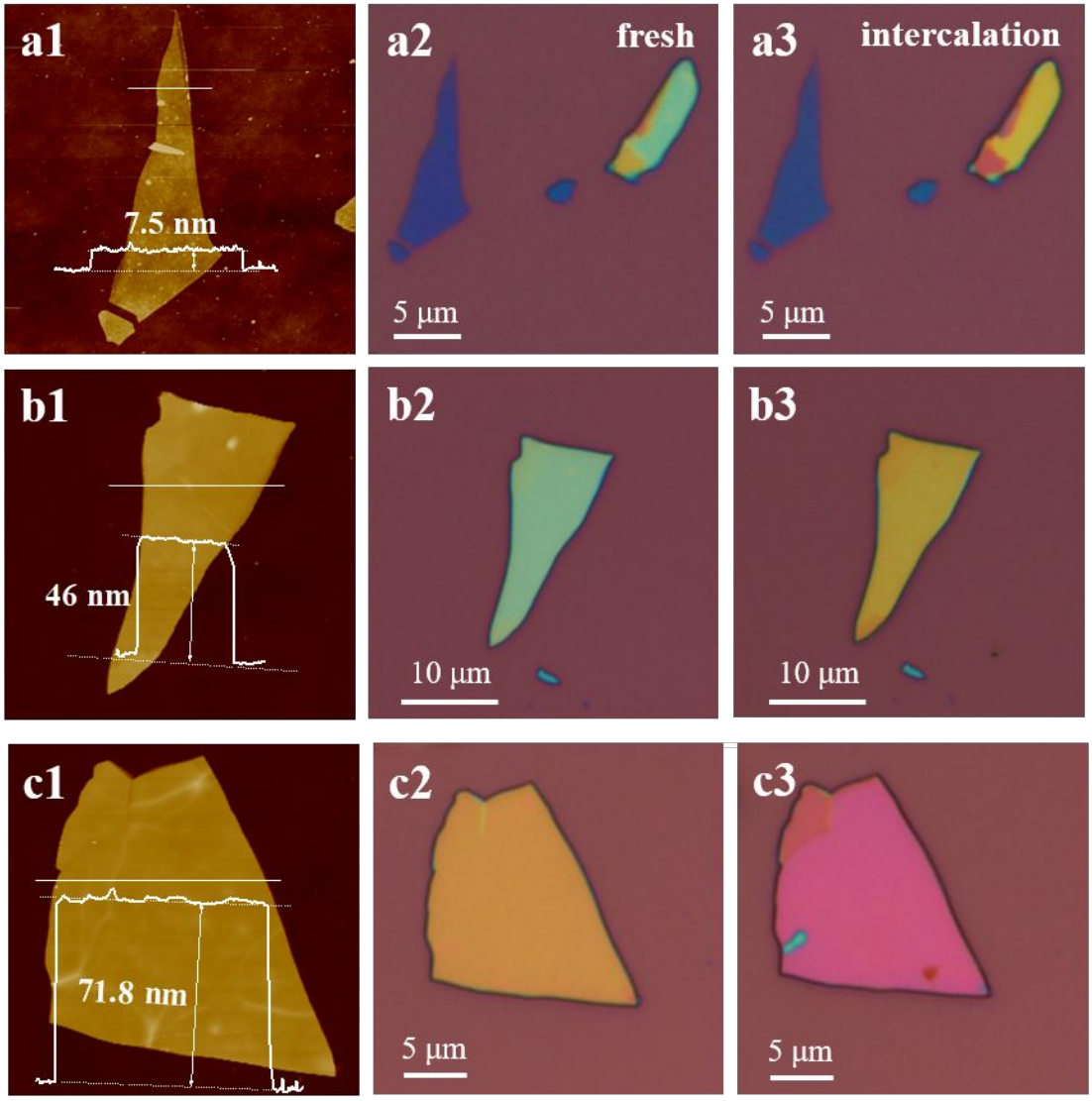

Figure S3. Optical micrographs corresponding to fresh and intercalation state of TaS_2 nanosheets with different thickness. (a1, a2, a3) 7.5 nm. (b1, b2, b3) 46 nm. (c1, c2, c3) 71.8 nm. Different size [Figure S2, Supporting Information (SI)] and thickness (Figure 3, SI) of TaS_2 nanosheets are tested and behave the similar change, and as the thickness increases, the change in color is more distinctive, indicating the universality of this intercalation method.

S4. XRD patterns of intercalated TaS_2 bulk crystal.

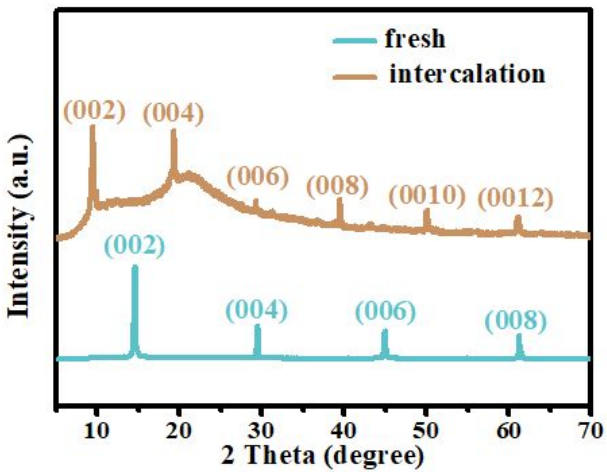

Figure S4. **XRD corresponding to fresh and intercalation state of TaS_2 bulk crystal.** XRD patterns of TaS_2 bulk crystal entirely shift toward low angel direction after intercalation, the peak corresponding to the (002) crystal plane shifts from 14.65 degrees to 9.56 after intercalation, suggesting that the interlayer spacing increases from 6.04 to 9.25 Å, similar with that of TaS_2 nanosheet, indicating the universality of this intercalation method including bulk form.

S5. The OM and AFM evolution of two individual nanosheets with intercalation of different amount of hydrazine.

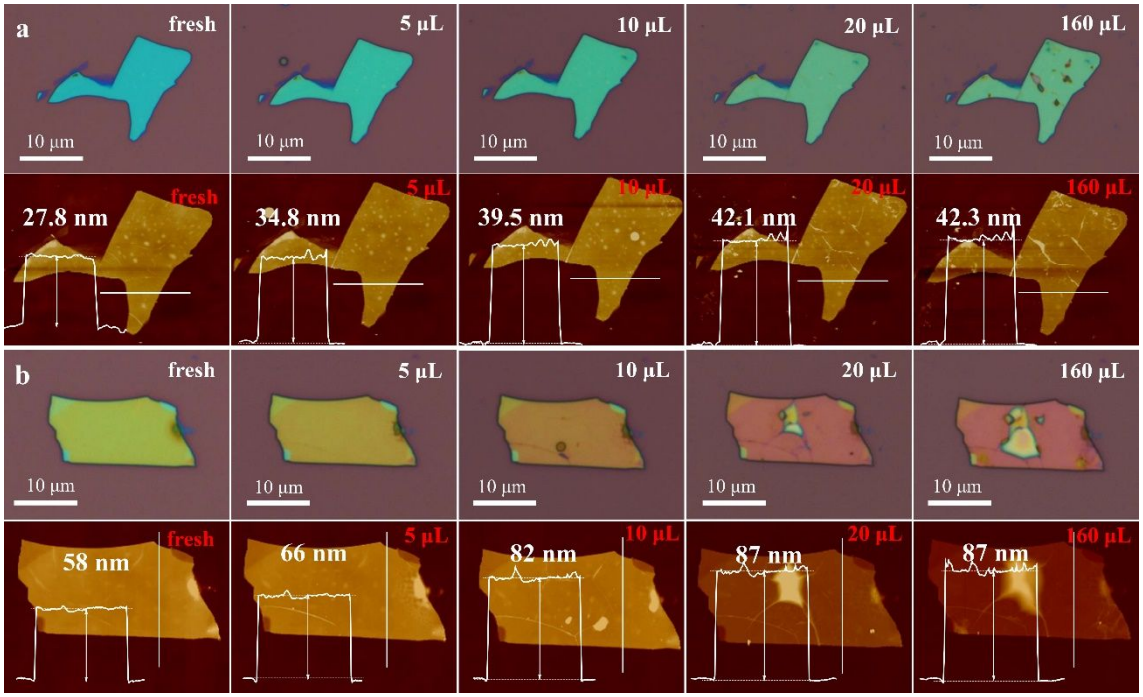

Figure S5. The OM and AFM evolution of two individual nanosheets with intercalation of different amount of hydrazine. As shown in Fig S4, the color changes as the amount of hydrazine increases. Taking the nanosheet in Figure S5a for example, the thickness is 58 nm in fresh state. Soaked in 5 μL hydrazine, the thickness is 66 nm and soaked in 10 μL hydrazine the thickness is 82 nm. The increased thickness in different states suggests the increased amount of intercalated N_2H_4, which is in positive correlation with the amount of hydrazine. When the concentration of hydrazine hydrate was the 160 μL used in our manuscript, N_2H_4 in the interlayer tended to be saturated and the interlayer distance expands to about 1.5 times. In other words, the ratio of the intercalated N_2H_4 can be adjusted conveniently by the concentration of hydrazine.

S6. The Raman spectroscopy with intercalation of different amount of hydrazine.

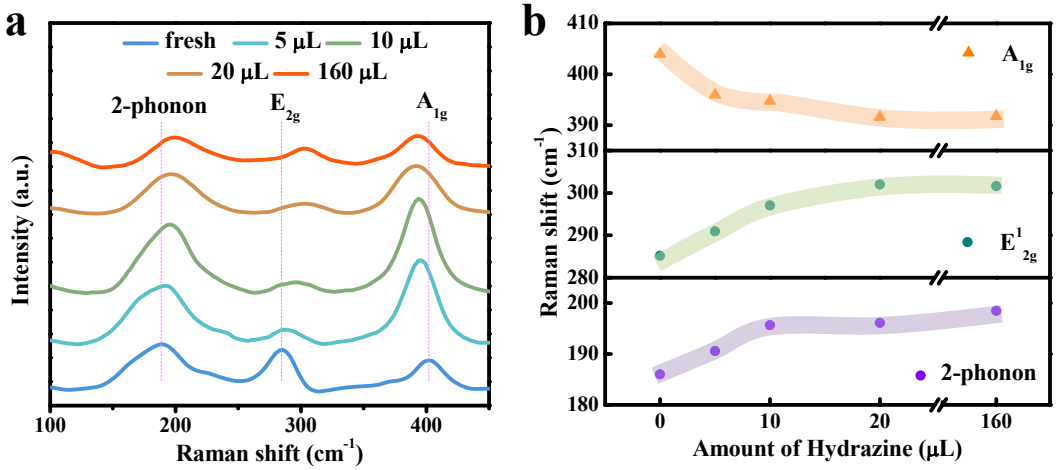

Figure S6. The Raman spectroscopy with intercalation of different amount of hydrazine.

Raman spectra can reflect the interlayer force and then indirectly reflects the layer spacing changes. The peaks of E^1_{2g} and 2-phonon behave "blue shift" and the peak of A_{1g} behaves "red shift" as the thickness increases, which derived from the weaked interlaminar force as inter-layer expansion (*J. Am. Chem. Soc.* **2017**, 139, 4623-4626).

S7. The OM evolution of two nanosheets with different intercalation time

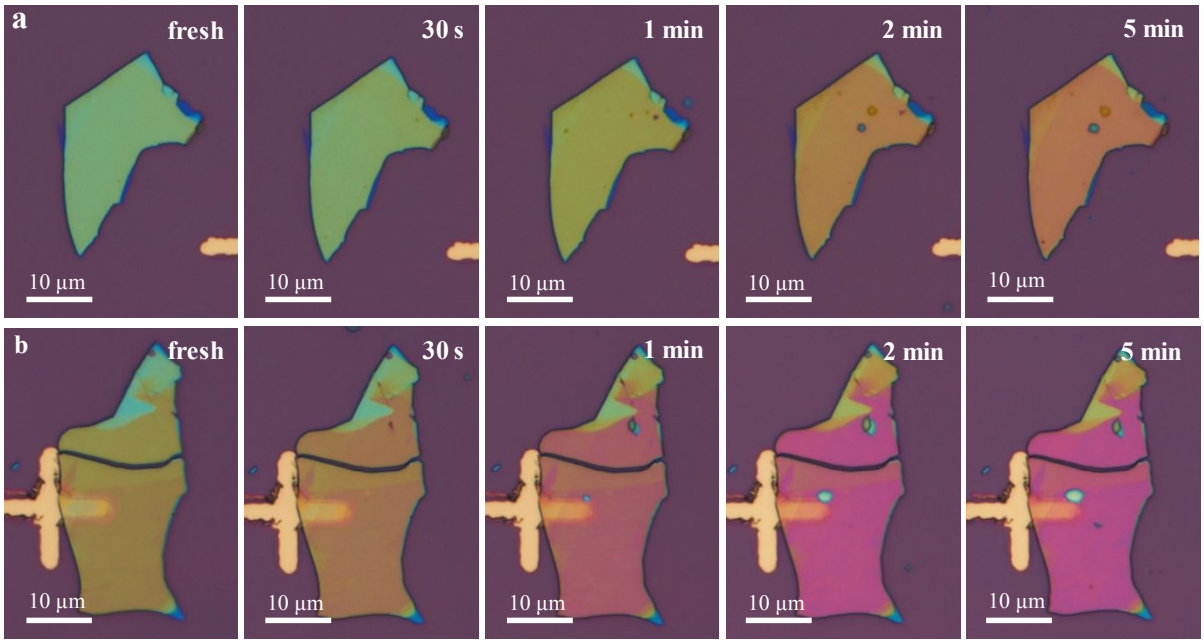

Figure S7. The OM evolution of two nanosheets with different intercalation time. In terms of the intercalation time, as shown in Fig R6, the color of nanosheet is in positive correlation with intercalation time. When the intercalation time is 5 min, the color change is negligible, suggesting the amount of N_2H_4 is saturated.

S8. The OM and AFM evolution of two individual nanosheets in air.

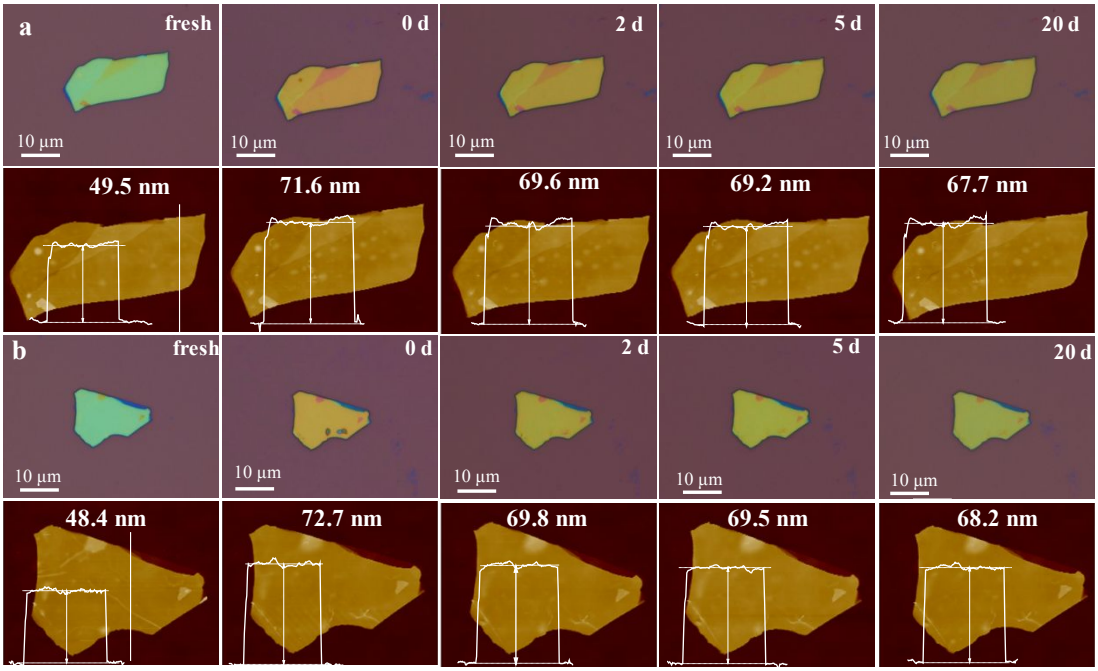

Figure S8. The OM and AFM evolution of two individual nanosheets in air. As shown in Figure S8, the slight change in thickness and color of a single superlattice flake after 20 days of placement indicates N_2H_4 molecules do not easily escape between layers. Meanwhile, negligible changes in surface morphology also show that the hybrid superlattice is relatively stable for resistance to oxidation. Satisfactory long-term stability in air of the hydrazine intercalated TaS_2 nanosheets may result from strong reducing property of N_2H_4.

S9. Elements mapping of N_2H_4-TaS_2 nanosheet.

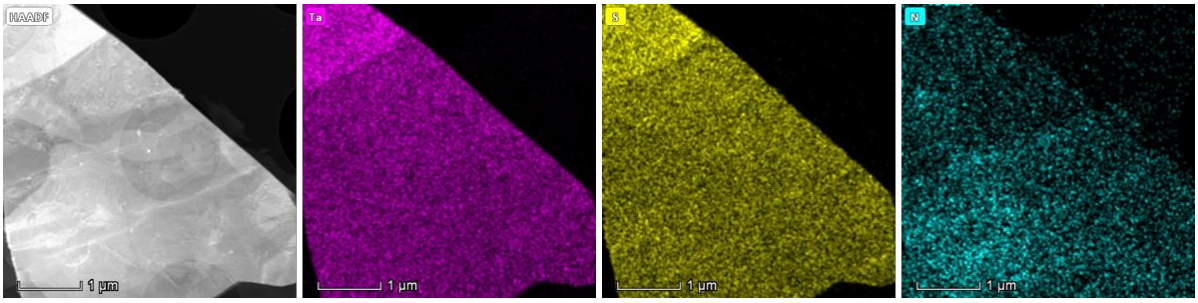

Figure S9. Elements mapping of another nanosheet shows the homogeneity of Ta and S elements and the existence of N element.

S10. Image of low magnification cross-sectional HAADF and the corresponding interlayer spacing in different regions.

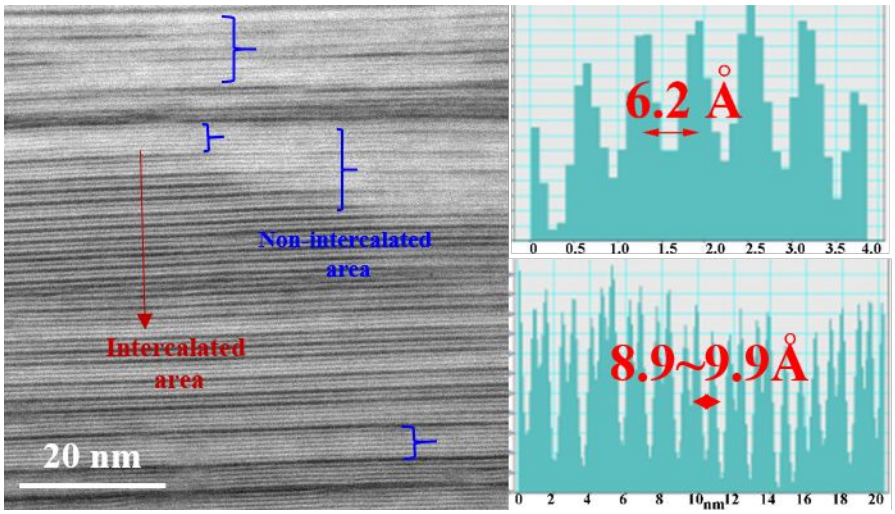

Figure S10. Image of low magnification cross-sectional HAADF and the corresponding interlayer spacing in different regions. The image shows the boundary line of intercalated and non-intercalated region and the change in interlayer spacing is more convincing comparing two regions.

S11. Cross-sectional HAADF images in different regions.

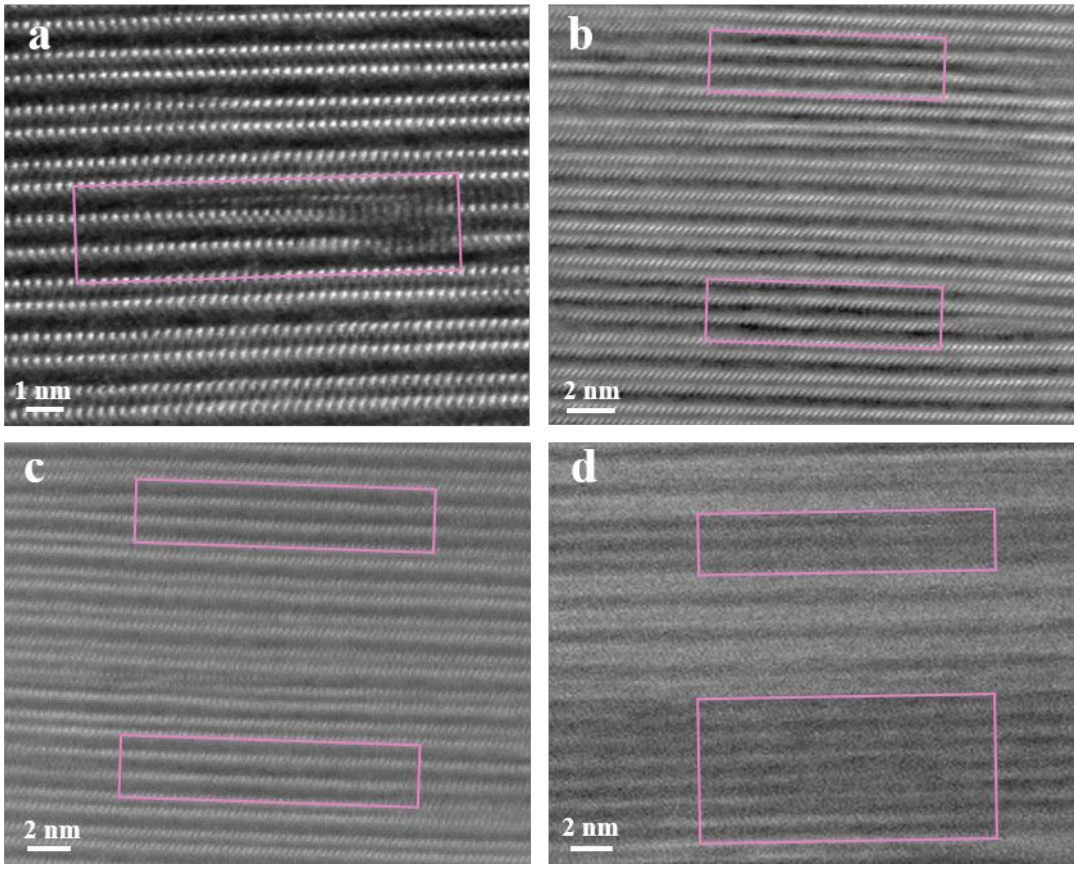

Figure S11. Cross-sectional HAADF images in different regions show that the intercalation changed from each layer to layer by layer under high energy electron beam radiation. A high-stage intercalation model in which two layers of TaS_2 are separated by one molecular layer existed in most regions (Figure 2e, Figure S6a-d). This results show that the molecules were not uniformly evaporated from the hybrid material during FIB cutting and high energy electron beam irradiation in cross- sectional HAADF imaging. It was shown that in the intercalation compounds, the molecules intercalated into a layered compound increases the strain energy by expanding the interlayer distance (*Nat. Commun.* **2017**, 8, 1024; *Adv. Phys*. **2002**, 51, 1). When there are too few molecules to fill in all the possible interlayer space, these molecules tend to aggregate to form clusters between a single set of the layers, rather than randomly and uniformly distribute in all the interlayer space, because this aggregation can reduce the strain energy of the whole system. Therefore, when most of the organic molecules are removed from the TaS_2-N_2H_4 hybrid material by vacuum heating, a random high-stage compound is formed to minimize the strain energy, as seen in Figure 2e.

S12. Thickness dependence of transition temperature of CDW in fresh TaS_2.

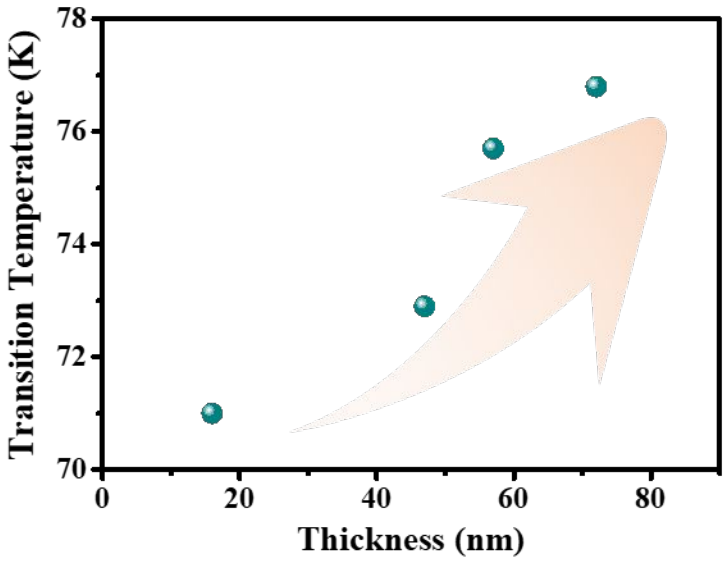

Figure S12. Thickness dependence of transition temperature of CDW in fresh TaS_2.

S13. The stability of intercalated N_2H_4 during reaction cycling

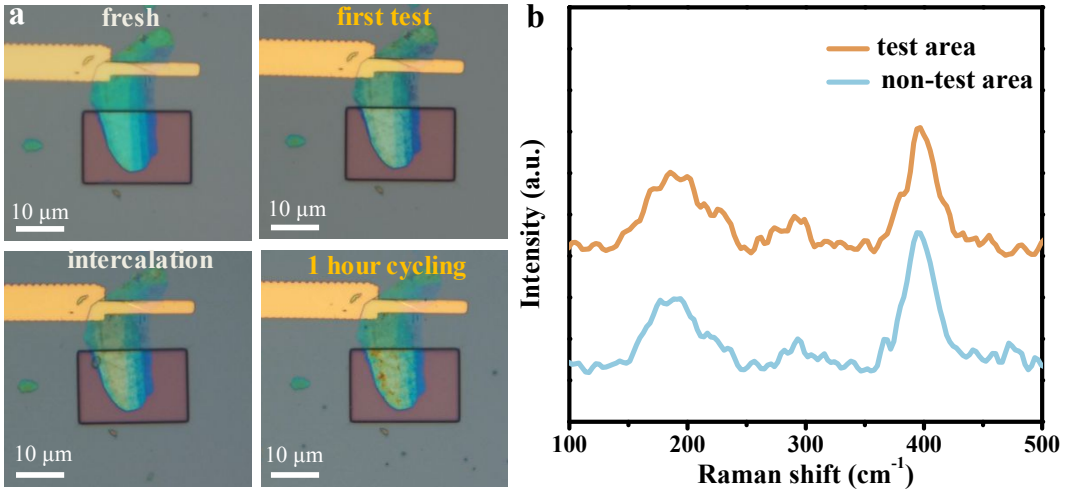

Figure S13. The stability of intercalated N_2H_4 during reaction cycling. (a) The OM of new electrochemical microcell under different states including fresh, first test, intercalation and 1 hour cycling. The devices kept intact, no crevices or pits are observed in the optical micrographs (OM) after reaction cycling of 1 hour, suggesting the stability of intercalated N_2H_4 during reaction cycling. (b) Raman spectroscopy of the test area and non-test area. The non-test area is coated with PMMA beside the test window on the nanosheet. The Raman spectroscopy of two kinds of regions maintain similar shapes and peak positions indicates the stability during testing.

S14. Electrocatalytic performance chart of tens of devices.

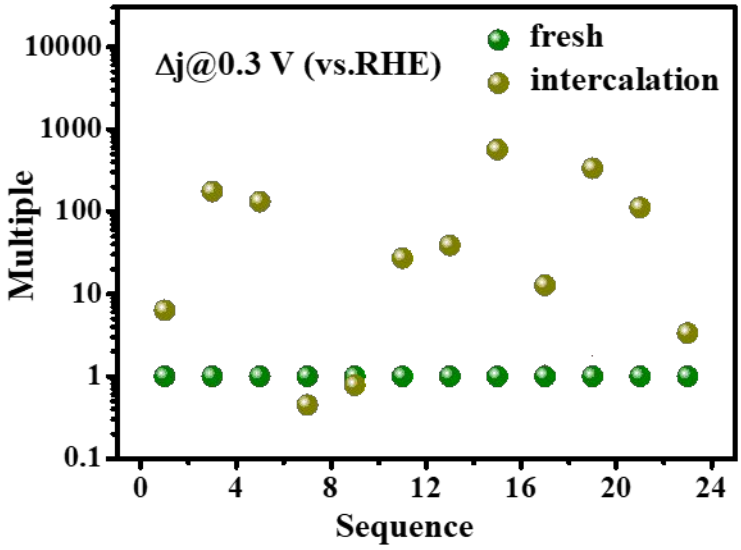

Figure S14. Electrocatalytic performance chart of tens of devices shows the repeatability and reliability of test. The polarization current of on-chip device is collected from a single catalyst, so the current is at the nA level in general. In this regard, the device current is susceptible to interference and repeatability and reliability appears especially important. In order to further prove that the enhanced performance is resulting from molecular interlayer rather than accidental factors, following Prof. Manish Chhowalla's work (Nat. Mater., 2016, 15, 1003.), we fabricated different batches of devices and make the final evaluation based on statistical law. Therefore, we have fabricated 10 individual devices and tested the performance of each individual device before and after intercalation. Figure S14 revealed the performance of the intercalated nanosheet is significantly improved compared with that of the fresh nanosheet for each individual device.

Table S1. Comparison on HER performances of 2D TaS_2 with other 2D TMDCs through microscale measurement

Catalyst	Measurement set-up	Overpotential @10mA/cm^2	Tafel Slope	References
2H-MoS_2	On-chip electrocatalytic microdevice	286	70	*Nat. Mater.*[1]
1T'-MoS_2		205	51	
2H-MoS_2		420	61-116	*Adv. Mater.*[2]
1T'-MoS_2		300	53-83	
1T'-MoS_2		191-199	142-148	*Adv. Mater.*[3]
WS_2		208	108	*Nat. Mater.*[4]
1T-VSe_2		126	70	*Nano Lett.*[5]
2H-TaS_2		280	111	*Mater. Today*[6]
3R-NbS_2		182	97	
WTe_2		300-410	110-141	*Adv. Mater.*[7]
2H-TaS_2		159-370	76-127	This work

Note: It is noticeable the exposed reactive areas, the position and electrode contact all seem to influence the absolute values of current density in this on-chip electrocatalytic microdevice. Therefore, performance comparisons on the same device may be more meaningful and reliable.

Table S2. Comparison on HER performances of 2D TaS_2 with the reported TaS_2 based materials through macroscale measurement.

Catalyst	Measurement set-up	Overpotential @10mA/cm^2	Tafel Slope	References
2H-TaS_2	Traditional test on glassy carbon electrode/ current collector	60	37	*Nat. Energy* [8]
2H-TaS_2		480	104.4	*J. Phys. Chem. C* [9]
1T-TaS_2		564	135	*Adv. Mater.* [10]
TaS_2		320	114.66	*J. Phys. Chem. C* [11]
2H-TaS_2/Au foils		65	33-42	*Nat. Commun.* [12]
1T-TaS_2/Au foils		205	67-82	*Adv. Mater.* [13]
$Pd_{0.1}TaS_2$		114	52.7	*J. Mater. Chem. A* [14]
Pt-TaS_2		190	54	*Energy Environ. Sci.* [15]
2H-TaS_2		159-370	76-127	This work

References

1. Liu, L.; Wu, J.; Wu, L.; Ye, M.; Liu, X.; Wang, Q.; Hou, S.; Lu, P.; Sun, L.; Zheng, J.; Xing, L.; Gu, L.; Jiang, X.; Xie, L.; Jiao, L. Phase-Selective Synthesis of 1T′ MoS_2 Monolayers and Heterophase Bilayers. *Nat. Mater.* **2018**, 17, 1108–1114.
2. Zhang, J.; Wu, J.; Guo, H.; Chen, W.; Yuan, J.; Martines, U.; Gupta, G.; Mohite, A.; Ajayan, P. M.; Lou, J. Unveiling Active Sites for the Hydrogen Evolution Reaction on Monolayer MoS_2. *Adv. Mater.* **2017**, 29, 1701955.
3. Nam, G. H.; He, Q.; Wang, X.; Yu, Y.; Chen, J.; Zhang, K.; Yang, Z.; Hu, D.; Lai, Z.; Li, B.; Xiong, Q.; Zhang, Q.; Gu, L.; Zhang, H. In-Plane Anisotropic Properties of 1T′-MoS_2

Layers. *Adv. Mater.* **2019**, 31, 1807764.

4. He, Y.; He, Q.; Wang, L.; Zhu, C.; Golani, P.; Handoko, A. D.; Yu, X.; Gao, C.; Ding, M.; Wang, X.; Liu, F.; Zeng, Q.; Yu, P.; Guo, S.; Yakobson, B. I.; Wang, L.; She, Z. W.; Zhang, Z.; Wu, M.; Wang, Q., *et al.* Self-Gating in Semiconductor Electrocatalysis. *Nat. Mater.* **2019**, 18, 1098–1104.
5. Yan, M.; Pan, X.; Wang, P.; Chen. F.; He, L.; Jiang, G.; Wang, J.; Liu, J. Z.; Xu, X.; Liao, X.; Yang, J.; Mai, L. Field-Effect Tuned Adsorption Dynamics of VSe_2 Nanosheets for Enhanced Hydrogen Evolution Reaction. *Nano Lett.* **2017**, 17, 4109–4115.
6. Zhang, J.; Wu, J.; Zou, X.; Hackenberg, K.; Zhou, W.; Chen, W.; Yuan, J.; Keyshar, K.; Gupta, G.; Mohite, A.; Ajayan, P. M.; Lou, J. Discovering Superior Basal Plane Active Two-Dimensional Catalysts for Hydrogen Evolution. *Mater. Today* **2019**, 25, 28.
7. Zhou, Y.; Silva, J. L.; Woods, J. M.; Pondick, J. V.; Feng, Q.; Liang, Z.; Liu, W.; Lin, L.; Deng, B.; Brena, B.; Xia, F.; Peng, H.; Liu, Z.; Wang, H.; Araujo, C. M.; Cha, J. J. Revealing the Contribution of Individual Factors to Hydrogen Evolution Reaction Catalytic Activity. *Adv. Mater.* **2018**, 30, 1706076.
8. Liu, Y.; Wu, J.; Hackenberg, K. P.; Zhang, J.; Morris Wang, Y.; Yang, Y.; Keyshar, K.; Gu, J.; Ogitsu, T.; Vajtai, R.; Lou, J.; Ajayan, P. M.; Wood, B. C.; Yakobson, B. I. Self-Optimizing, Highly Surface-Active Layered Metal Dichalcogenide Catalysts for Hydrogen Evolution. *Nat. Energy* **2017**, 2, 17127.
9. Feng, Y.; Gong, S.; Du, E.; Chen, X.; Qi, R.; Yu, K.; Zhu, Z. 3R TaS_2 Surpasses the Corresponding 1T and 2H Phases for the Hydrogen Evolution Reaction. *J. Phys. Chem. C* **2018**, 122, 2382–2390.
10. Li, H.; Tan, Y.; Liu, P.; Guo, C.; Luo, M.; Han, J.; Lin, T.; Huang, F.; Chen, M. Atomic-Sized Pores Enhanced Electrocatalysis of TaS_2 Nanosheets for Hydrogen Evolution. *Adv. Mater.* **2016**, 28, 8945–8949.
11. Nguyen, T. P.; Choi, S.; Jeon, J. M.; Kwon, K. C.; Jang, H. W.; Kim, S. Y. Transition Metal Disulfide Nanosheets Synthesized by Facile Sonication Method for the Hydrogen Evolution Reaction. *J. Phys. Chem. C* **2016**, 120, 3929–3935.
12. Shi, J.; Wang, X.; Zhang, S.; Xiao, L.; Huan, Y.; Gong, Y.; Zhang, Z.; Li, Y.; Zhou, X.; Hong, M.; Fang, Q.; Zhang, Q.; Liu, X.; Gu, L.; Liu, Z.; Zhang, Y. Two-Dimensional Metallic Tantalum Disulfide as a Hydrogen Evolution Catalyst. *Nat. Commun.* **2017**, 8,

958.

13. Huan, Y.; Shi, J.; Zou, X.; Gong, Y.; Zhang, Z.; Li, M.; Zhao, L.; Xu, R.; Jiang, S.; Zhou, X.; Hong, M.; Xie, C.; Li, H.; Lang, X.; Zhang, Q.; Gu, L.; Yan, X.; Zhang, Y. Vertical 1T-TaS_2 Synthesis on Nanoporous Gold for High-Performance Electrocatalytic Applications. *Adv. Mater.* **2018**, 30, 1705916.
14. Wang, D.; Wang, X.; Lu, Y.; Song, C.; Pan, J.; Li, C.; Sui, M.; Zhao, W.; Huang, F. Atom-Scale Dispersed Palladium in a Conductive $Pd_{0.1}TaS_2$ Lattice with a Unique Electronic Structure for Efficient Hydrogen Evolution. *J. Mater. Chem. A* **2017**, 5, 22618–22624.
15. Zeng, Z.; Tan, C.; Huang, X.; Bao, S.; Zhang, H. Growth of Noble Metal Nanoparticles on Single-Layer TiS_2 and TaS_2 Nanosheets for Hydrogen Evolution Reaction. *Energy Environ. Sci.* **2014**, 7, 797–803.